Localisation of a Stationary Time-Harmonic Dipole Sound Source in Flows using Time-Reversal Simulation

A. Mimani (1), C. J. Doolan (1) and P. R. Medwell (1)

(1) School of Mechanical Engineering, The University of Adelaide, South Australia 5005, Australia

ABSTRACT

This work analyses the accuracy of numerical Time-Reversal (TR) simulations implemented using two different Time-Reversal Mirror (TRM) configurations for localising and characterising a stationary acoustic dipole source in a mean flow. The forward time evolution of the acoustic fields is simulated by means of the numerical solution of the inhomogeneous 2-D Linearised Euler Equations (LEE) with uniform subsonic mean flow. Only the acoustic pressure is recorded with two line arrays (LAs) of boundary nodes in a TRM corresponding to the top and bottom boundaries. The time-reversed acoustic pressure history is used as input data for simulating two numerical TR experiments; (a) one line array (LA) in a TRM corresponding to the top boundary and (b) two LAs in a TRM corresponding to the top and bottom boundaries. The Root-Mean-Square (RMS) of the time-reversed acoustic pressure field obtained by the first experiment indicates only one spatial maxima region (focal spot), therefore incorrectly suggests that the source is a monopole, whereas the second experiment correctly reveals the source to be a dipole. The local acoustic pressure history at two source locations is shown to be coherent with relative phase exactly equal to π radian, thereby confirming the dipole source nature. This demonstrates that two LAs in a TRM located on either sides of the mean flow are required to take into consideration, the complete phase information and thereby accurately characterise a dipole.

INTRODUCTION

Time-Reversal (TR) simulations implemented using a limited angular aperture line array (LA) in a Time-Reversal Mirror (TRM) has a limited reversal and focusing quality for localising a source region (Fink and Prada, 2001) because only a small fraction of the acoustic pressure radiated (and not complete field information) may be recorded. However, a microphone LA configuration in a TRM completely enclosing the source intercepts the acoustic wave propagating in all the directions (Fink and Prada, 2001, Fink *et al*. 2000), thereby revealing the most accurate prediction of source location and the source characteristics such as shape and strength of a pulse from numerical TR simulations (Deneuve *et al*. 2010, Fink *et al*. 2000). However, the implementation of such a LA configuration in an aeroacoustics experiment is difficult experimentally due to the number of microphones required and/or because the microphone locations may be restricted to regions outside the flow field.

Padois *et al*. (2012) use acoustic pressure time-history measured over one LA of microphones in a TRM (located outside the shear flow) to localise time-harmonic aeroacoustic sources such as a monopole source (modelled by a speaker) and dipole source (modelled by two speakers out-of phase with each other) in wind tunnel flows using TR simulations based on numerical solution of the 2-D Linearised Euler Equations (LEE) using central Dispersion-Relation-Preserving Finite-Difference (FD) schemes (Tam and Webb, 1993). In the case of Padois *et al*. (2012), the dipole axis was parallel to the flow direction. The predicted location of source(s) was given by maxima point of the focal spot(s) in the spatial distribution of time-reversed square-pressure field. The geometrical centre of the two sources predicted by the time-reversed square-pressure field was taken as the predicted location of the dipole source and this was found to be in satisfactory agreement with the known source position. Furthermore, the dipole source nature was established by showing a π radian phase jump in the phase distribution of the acoustic pressure time-history across the line passing through the geometrical centre of the predicted dipole source location. It is however, noted that the practically relevant cases of a dipole source with axis perpendicular to the flow (modelled by a uniform cylinder in mean flow with axis perpendicular to flow direction, (Blake, 1986)) or a lateral quadrupole source (such as free turbulence) were not considered.

The main limitation in the work of Padois *et al*. (2012) is the use of one LA in a TRM (located at the top boundary of the wind tunnel) which cannot record sufficient acoustic pressure time-history data to properly characterise a dipole source with its axis perpendicular to the flow. The out-of phase radiation pattern about the mean flow direction signifies that one LA in a TRM can capture only half the phase information, and therefore, would incorrectly predict a monopole source. Indeed, one LA in a TRM would also be unable to characterise higher-order sources such as a lateral and longitudinal quadrupole source. Another drawback in the numerical simulations of Padois *et al*. (2012) is the computation of Fourier Transform to obtain the phase information of the local acoustic pressure over the entire computational domain which can be computationally expensive for large domains.

Deneuve *et al*. (2010) examined the completeness of boundary data (i.e., the use of multiple line arrays (LAs) in a TRM) on the accuracy of source localisation in a 2-D rectangular domain by means of numerical TR simulations based on the Pseudo-Characteristic Formulation (PCF) (Sesterhenn, 2001) and overall upwind biased Finite-Difference (FD) schemes (Li and Sagaut, 2007). However, this analysis was confined to the case of an idealised Gaussian pulse. Their TR simulations also make use of the time-reversed velocity histories (in addition to time-reversed pressure history) which can be easily stored during numerical forward simulations but are typically difficult to measure experimentally. Nonetheless, it was noted that the location of the initial emission point of the pulse was satisfactorily predicted regardless of the number of LAs used; thereby suggesting that a reasonable estimate of the location of aeroacoustic sources may be obtained using a

single LA in a TRM. However, the shape and strength of the pulse obtained using one LA in a TRM are significantly different from the pulse at the initial time-instant during forward simulations which hints at use of multiple LAs for characterising aeroacoustic sources. Recently, Harker and Anderson (2013) obtained an optimised TRM layout in terms of the angular spacing and aperture of a LA of microphones located on a circular arc for localising a time-harmonic simple (monopole) source in a stationary medium.

This paper investigates what effect using more than one LA in a TRM has on the accuracy of the localisation and characterisation of higher-order aeroacoustic sources, such as a harmonic dipole source with its axis perpendicular to the flow. The objectives of this work are then to conduct numerical experiments to (1) first establish the improvement in accuracy of the predicted source location using two LAs, (2) demonstrate that the use of two LAs is sufficient for confirming the monopole or dipole source characteristics and (3) suggest a simple method to find the relative phase between the acoustic pressure time-history at the predicted focal point locations to confirm the dipole source nature. The computational advantage of this method to obtain the relative phase is that it avoids the unnecessary computation of Fourier Transform over the entire domain; rather the dipole source nature may be confirmed by simply computing the time-lag of the coherent acoustic pressure time-history at the two focal points. The practical importance of the simulation results is seen in obtaining guidelines (in terms of the objective (2)) for designing an experiment involving acoustic pressure measurements over microphone LAs in a TRM located at the boundaries of an anechoic wind tunnel.

IMPLEMENTATION OF NUMERICAL SIMULATIONS: METHODOLOGY

Forward Simulations

An algorithm for the numerical implementation of forward and TR simulation of the inhomogeneous 2-D LEE assuming homoentropic flow conditions on a rectangular computational domain given by $-L_y \le y \le L_y, -L_x \le x \le L_x$ is briefly described. To this end, the inhomogeneous 2-D LEE are recast in the PCF (Sesterhenn, 2001) as:

$$\frac{\partial}{\partial t}\begin{Bmatrix}\widetilde{p}\\ \widetilde{u}\\ \widetilde{v}\end{Bmatrix}=\begin{Bmatrix}-\dfrac{\rho_0 c_0}{2}\left\{\left(X^{+}_{\text{linear}}+X^{-}_{\text{linear}}\right)+\left(Y^{+}_{\text{linear}}+Y^{-}_{\text{linear}}\right)\right\}\\ -\dfrac{1}{2}\left(X^{+}_{\text{linear}}-X^{-}_{\text{linear}}\right)\\ -\dfrac{1}{2}\left(Y^{+}_{\text{linear}}-Y^{-}_{\text{linear}}\right)-c_0 M_0\dfrac{\partial\widetilde{v}}{\partial x}\end{Bmatrix}+\{\mathbf{S}\}, \quad (1a, b, c)$$

where

$$X^{\pm}_{\text{linear}}=\pm c_0\left(1\pm M_0\right)\left\{\frac{1}{\rho_0 c_0}\frac{\partial\widetilde{p}}{\partial x}\pm\frac{\partial\widetilde{u}}{\partial x}\right\},$$
$$Y^{-}_{\text{linear}}=\pm c_0\left\{\frac{1}{\rho_0 c_0}\frac{\partial\widetilde{p}}{\partial y}\pm\frac{\partial\widetilde{v}}{\partial y}\right\}. \quad (2, 3)$$

In Eqs. (1-3), ρ_0 is the ambient density, $\widetilde{p}(x,y,t)$, $\widetilde{u}(x,y,t)$ and $\widetilde{v}(x,y,t)$ are the acoustic pressure, acoustic particle velocities along the *x* and *y* directions, respectively, c_0 is the uniform sound speed (under isentropic conditions), M_0 is the subsonic uniform mean flow Mach number along the positive *x* direction, *t* represents the forward time. $X^{\pm}_{\text{linear}}$ denote fluxes propagating along the positive and negative *x* directions, respectively, whilst $Y^{\pm}_{\text{linear}}$ denote fluxes propagating along the positive and negative *y* directions, respectively. The vector $\{\mathbf{S}\}$ modelling aeroacoustic sources such as idealised monopole and dipole sources is adopted from Bailly and Juve (2000). A monopole source is modelled by

$$\{\mathbf{S}\}=c_0^2\rho_0 Q_0\,\delta(x-x_m)\delta(y-y_m)\sin(\omega t)\times\{1\quad 0\quad 0\}^T, \quad (4)$$

where Q_0 and (x_m, y_m) represents the strength and location of the source, respectively, whilst $\omega=2\pi\cdot f$ is the angular frequency (in radian $\cdot\,\text{s}^{-1}$) and f is the frequency in Hertz. An idealised dipole source (located on the *y* axis) with axis perpendicular to mean flow is modelled by

$$\{\mathbf{S}\}=\sin(\omega t)\times\{0\quad 0\quad(\varepsilon_d/\rho_0)\cos(\alpha_d y)\}^T, \quad (5)$$

where $|y|\le y_d$ and ε_d denotes amplitude of the fluctutaing force. Moreover, α_d is chosen such that the geometrical centre of the dipole source is at origin. The computational domain is discretized into equally spaced N_x and N_y nodes along the *x* and *y* directions, respectively, so that the total number of nodes is given by $N_y \times N_x$. The mesh sizes along *x* and *y* directions are given by $\Delta x = 2L_x/(N_x-1)$ and $\Delta y = 2L_y/(N_y-1)$, respectively. The spatial derivatives in fluxes propagating along the positive $\left(X^{+}_{\text{linear}}, Y^{+}_{\text{linear}}\right)$ and negative $\left(X^{-}_{\text{linear}}, Y^{-}_{\text{linear}}\right)$ directions are computed using overall upwind biased FD schemes implemented as matrix-column multiplication shown as

$$\frac{\partial\{\psi\}^{+}}{\partial n}\approx\frac{1}{\Delta n}[\mathbf{R}_1]\{\psi\},\quad \frac{\partial\{\psi\}^{-}}{\partial n}\approx\frac{1}{\Delta n}[\mathbf{R}_2]\{\psi\}, \quad (6, 7)$$

respectively, where $\{\psi\}=\{\psi_1,\psi_2,\psi_3,\cdots,\psi_N\}^T$ represents either the acoustic pressure or the acoustic paticle velocities. $[\mathbf{R}_1]$ and $[\mathbf{R}_2]$ are the overall upwind biased FD scheme matrices formulated using (a) 4th order, 7-point optimised upwind biased FD scheme of Zhuang and Chen (2002) at interior nodes, (b) the 5th and 3rd order standard upwind biased FD schemes (Li, 1997) near the boundary nodes, (c) the 7-point optimised one-sided FD scheme (Zhaung and Chen, 2002) at the penultimate nodes and (d) the 7-point optimised backward FD scheme of Tam (1995) at the boundary nodes. It is noted that $\{\psi\}$ represents either the acoustic pressure or particle velocities, *N* stands for N_x or N_y and Δn represents Δx or Δy. Since the mean flow is assumed to be along the positive *x* direction, the spatial derivative $\partial\widetilde{v}/\partial x$ in Eq. (1c) is computed using Eq. (6). The 3rd order TVD Runge-Kutta scheme (Shu and Osher, 1988) is used for time-integration during forward and TR simulations. The time-step Δt in forward simulations is computed in accordance with

$$CFL=\frac{(1+M_0)c_0\Delta t}{\Delta n}\le 1. \quad (8)$$

In this work, however, a much smaller *CFL* number given by 0.05 is considered to ensure accuracy. The first-order Clayton-Engquist-Majda (CEM) anechoic boundary conditions (BC's) are implemented (Engquist and Majda, 1977, Clayton and Engquist, 1977) which is equivalent to set the incoming

flux to zero at boundaries $|x| = L_x$ and $|y| = L_y$ in the PCF of the 2-D LEE (Lu and Sagaut, 2007). In addition, the corner anechoic BC's proposed by Engquist and Majda (1979) was implemented at the four corner nodes of the rectangular computational domain. Furthermore, for the case of non-zero mean flow along the positive *x* direction, the spatial derivative $\partial\tilde{v}/\partial x$ was set to zero at all the nodes on the $x = -L_x$ boundary to suppress the incoming flux and thereby prevent instability. The forward time simulation is implemented for a large time-interval $t = [0, T_{\max} = N_{\max}\Delta t]$ during which the zero-initial conditions were replaced with several periods of time-harmonic response over the entire domain.

TR Simulations

The acoustic pressure was stored at nodes of all four boundaries of computational domain, i.e. at $x = \pm L_x, |y| \le L_y$ (the left and right boundaries, respectively) and at $y = \pm L_y, |x| \le L_x$ (the top and bottom boundaries, respectively) during every time-step of the forward simulations. The stored acoustic pressure time-history were used as Dirichlet BC's at the boundary nodes during every discrete time-step of the numerical TR simulations which back-propagate the acoustic waves into the computational domain (Padois *et al*., 2012). The 2-D LEE for implementing the numerical TR simulation was obtained by setting $\{\mathbf{S}\} = 0$ in Eqs. (1a-c), reversing the mean flow direction, i.e., $M_0 \to -M_0$ and transforming the forward time *t* and state variables (Denuve *et al*., 2010, Padois *et al*., 2012) shown as

$$t \to T_{\max} - \tilde{t}, \quad \tilde{p}(x,y,t) \to \tilde{p}(x,y,\tilde{t}),$$

$$\tilde{u}(x,y,t) \to -\tilde{u}(x,y,\tilde{t}), \ \tilde{v}(x,y,t) \to -\tilde{v}(x,y,\tilde{t}). \qquad (9a\text{-}d)$$

Here, $\tilde{t}$ represents the reversed time. The numerical TR simulations are implemented by enforcing the time-reversed acoustic pressure data at nodes (after every step of time-integration) on either (1) one LA in a TRM located at the top $(y = L_y)$ boundary or on (2) two LAs in a TRM located at the top and bottom $(y = -L_y)$ boundaries. The acoustic particle velocity measurements are difficult experimentally (Padois *et al*., 2012). It is for this reason that during the numerical forward simulations (which substitutes experiment); the velocity time-histories were not recorded, thence not specified at the LA(s) during TR simulations. Rather, the acoustic particle velocity fields are allowed to evolve and the accuracy of TR simulations is investigated using only the time-reversed acoustic pressure history input at the LA(s), see Mimani *et al*., 2013(a). In addition, the first-order CEM anechoic BC's were implemented at nodes on all the four boundaries and the corner BC's were also implemented at four corners of the rectangular domain to eliminate the reflections due to fluxes impinging at the computational boundaries. During the TR simulations, $M_0 \to -M_0$, therefore, $\partial\tilde{v}/\partial x$ in the time-reversed momentum equation along the *y* direction was computed using Eq. (7) and to prevent instability, $\partial\tilde{v}/\partial x$ was set to zero at all the nodes on the $x = L_x$ boundary.

SIMULATION RESULTS AND DISCUSSION

The numerical simulations are carried out on the domain of half-length $L_x = L_y = 0.5\,\text{m}$ with $N_x = N_y = 101$ implying $\Delta x = \Delta y = 0.01\,\text{m}$. The sound speed c_0 and ambient density ρ_0 are taken as $343.14\,\text{m}\cdot\text{s}^{-1}$ and $1.21\,\text{kg}\cdot\text{m}^{-3}$, respectively. The time-harmonic aeroacoustic sources have frequency $f = 3000\,\text{Hz}$ and wavelength $\lambda = c_0/f = 0.1144\,\text{m}$. The 3rd order standard upwind biased FD scheme (Li, 1997) which has the least Dispersion-Relation-Preserving (DRP) characteristics $(\text{about } \alpha = 0.62)$ amongst all the FD schemes used and decides the maximum frequency that can be accurately propagated (without significant dispersion). Therefore, for the mesh size and c_0 considered, the maximum frequency resolution band (Tam and Webb, 1993) is determined by

$$f_{\text{FD}} = \left[0, \left(\frac{\alpha}{2\pi}\right)\left(\frac{c_0}{\Delta n}\right)\right] \approx \left[0, \left(\frac{0.62}{2\pi}\right)\left(\frac{343.14\,\text{m}\cdot\text{s}^{-1}}{0.01\,\text{m}}\right)\right] \approx [0,\ 3385]\,\text{Hz}. \qquad (10)$$

This warrants an accurate numerical forward and TR simulations. Furthermore, $M_0 = 0.3$ and $N_{\max} = 7000$ are considered for forward simulations, hence, $\Delta t = 1.1209 \times 10^{-6}$ s and $T_{\max} = 7.8461 \times 10^{-3}$ s.

Forward Simulations

Figures 1a and b depict instantaneous time-snapshots of the $\tilde{p}(x,y,t)$ field due to an idealised (a) monopole source (of strength $Q_0 = 1 \times 10^{-3}\ \text{m}^2\cdot\text{s}^{-1}$) simulated by a point source at $x = y = 0$ and (b) dipole source with axis perpendicular to flow or along the *y* direction simulated by a fluctuating force term[8] of amplitude $\varepsilon_d = 1\ \text{N}\cdot\text{m}^{-3}$, located on the *y* axis with $y_d = 0.02\,\text{m}$, and $\alpha_d = 25\pi$ (so that $\cos(\alpha_d |y_d|) = 0$), respectively, (Bailly and Juve, 2000) at $t = T_{\max}$ in uniform mean flow $M_0 = 0.3$ along the positive *x* direction. The geometrical centre of excitation domain is taken as the known location of these idealised monopole and dipole sources (x_s, y_s), therefore, $x_s = y_s = 0$ and is indicated by a circle **O** in Figs. 1a and b, and also in the subsequent figures. (The colourbar shows the acoustic pressure in Pa.) The convective mean flow effect in Figs. 1a and b is observed by noting that the apparent wavelength of acoustic waves propagating towards the positive and negative *x* directions is $\lambda_c^{\pm} = (1 + M_0)\lambda$, respectively, (Bailly and Juve, 2000) as a result, acoustic pressure contours of the monopole source are elliptical, rather than circular. Moreover, the acoustic pressure contours of the dipole source are also not symmetric about the *y* axis. Nonetheless, the contours in acoustic pressure field of the dipole source have exactly opposite phases about the *x* axis; hence, the nodal line in Fig. 1b is oriented along the *x* axis. The directivity in acoustic pressure field of the dipole source is attributed to two simple sources of equal magnitude but exactly opposite phase located at $(x_{s_1}, y_{s_1}) = (0,\ 0.02\,\text{m})$ and $(x_{s_2}, y_{s_2}) = (0, -0.02\,\text{m})$ as may be observed from Fig. 1b. Given the location of sources at origin and diminished speed $c_0(1 - M_0)$ of waves propagating along the negative *x* direction, the time-harmonic response is developed when the wave fronts intercept the $x = -0.5\,\text{m}$ boundary at the very first instance, which evaluates to $t \approx 1858\,\Delta t$. Hence, the time corresponding to development of a time-harmonic response is taken as $t = T_{\text{steady}} = 2000\,\Delta t$ for implementing the TR simulations.

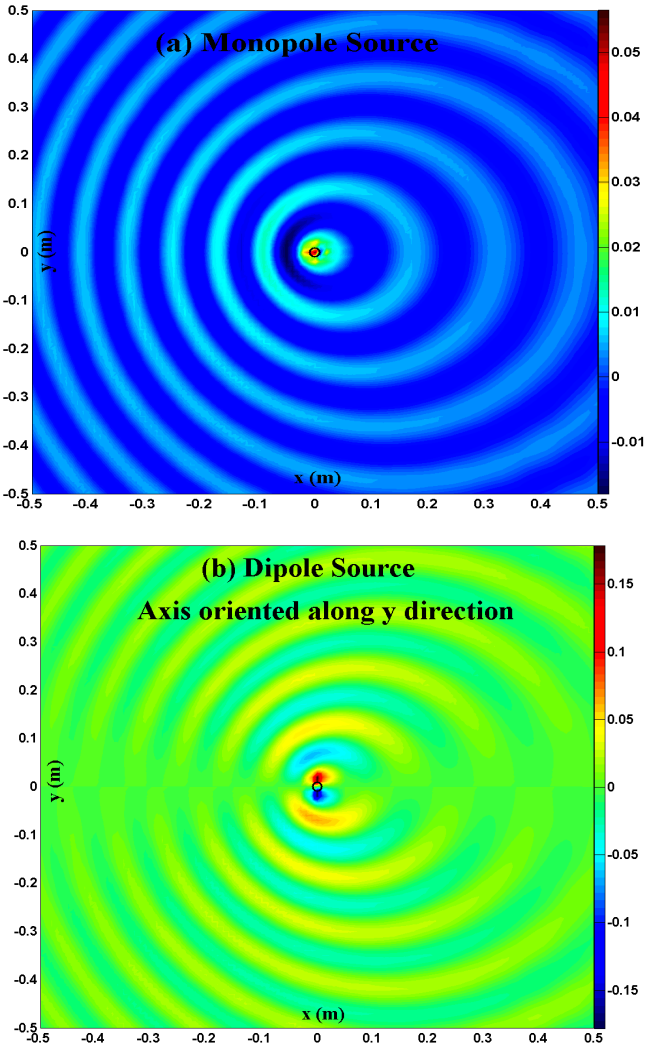

Figure 1 Forward simulation of the acoustic pressure field at $t = 7000\Delta t$ due to an idealised (**a**) Monopole source and (**b**) Dipole source (axis oriented along the y direction) located at origin in uniform subsonic mean flow $M_0 = 0.3$ along the positive x direction.

TR Simulations using one LA and two LAs in a TRM

Figures 2a and b shows time-snapshots of acoustic pressure field at $\tilde{t} = 1200\,\Delta t$ and $\tilde{t} = 3645\,\Delta t$, respectively, illustrating the back-propagation of acoustic waves into the computational domain from one LA located at $y = 0.5$ m boundary during TR simulations of a dipole source.

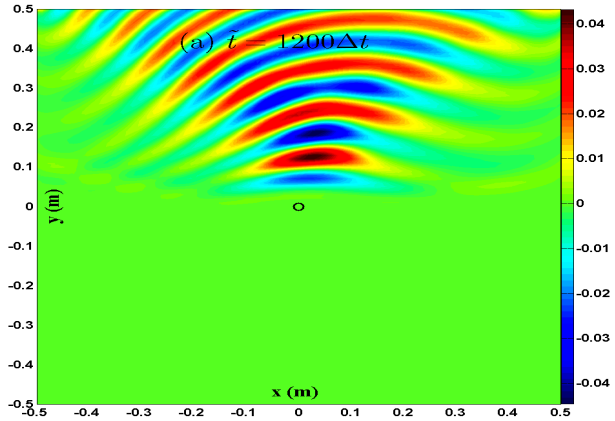

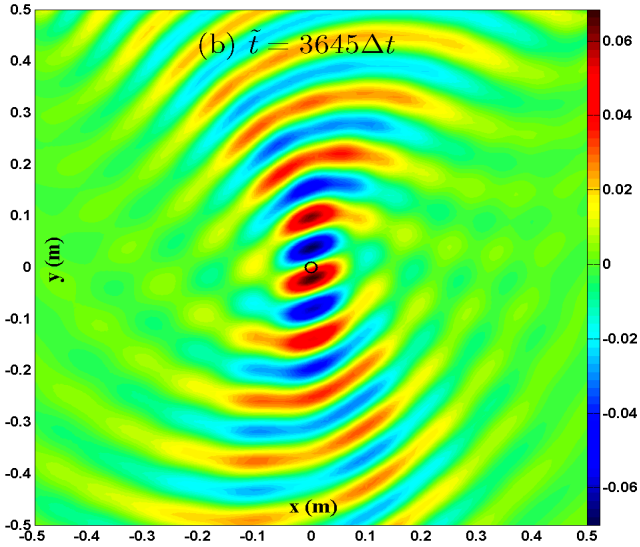

Figure 2 Time-snapshots of $\tilde{p}(x, y, \tilde{t})$ field obtained during TR simulations for localising a dipole source using a TRM comprising of one LA located at $y = 0.5$ m boundary for (a) $\tilde{t} = 1200\,\Delta t$ and (b) $\tilde{t} = 3645\,\Delta t$.

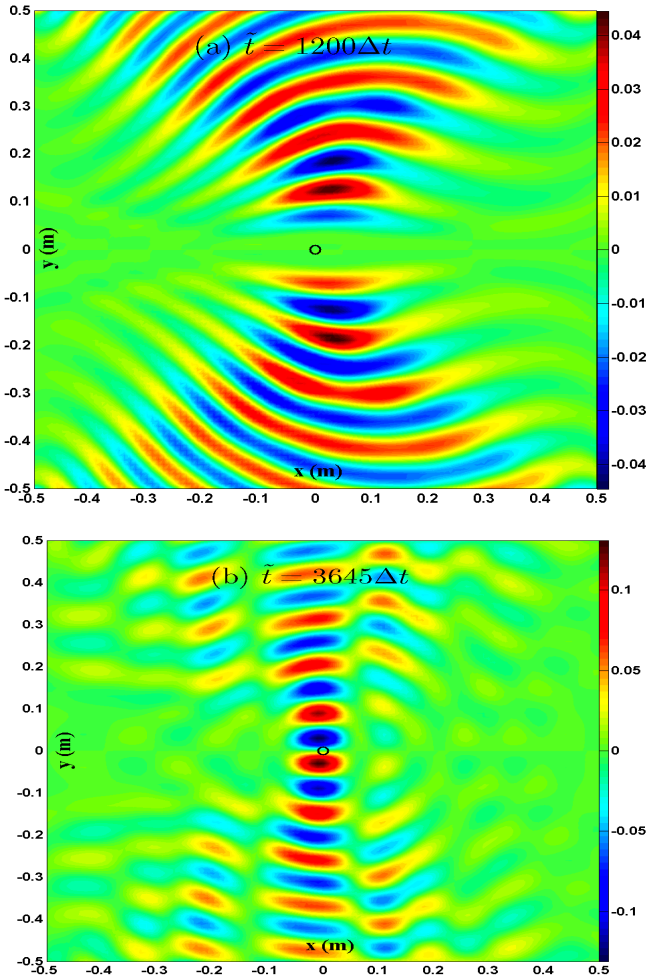

Figure 3 Time-snapshots of $\tilde{p}(x, y, \tilde{t})$ field obtained during TR simulations for localising a dipole source using a TRM comprising of two LAs located at $y = \pm 0.5$ m boundaries for (a) $\tilde{t} = 1200\,\Delta t$ and (b) $\tilde{t} = 3645\,\Delta t$.

The corresponding acoustic pressure field obtained using two LAs located at $y = \pm 0.5$ m boundaries are shown in Figs. 3a and b, respectively. It is observed in Fig. 2a that the acoustic waves emanating from the LA at top boundary are about to pass through the known dipole source region (i.e., at the origin). The width of the wave front has decreased whilst their amplitudes increased significantly near the source region (Padois *et al*., 2012). In Fig. 2b, the acoustic waves have passed through and diverged from the source region (due to absence of a sink, Bavu *et al*., 2007) with their width increased and amplitudes decreased substantially. These wave fronts gradually leave the computational boundaries without suffering reflections due to enforcement of anechoic BC's. On the other hand, Fig. 3a shows the acoustic waves emanating from two LAs at $y = \pm 0.5$ m boundaries are about to simultaneously arrive at the dipole source region wherein similar changes in width and amplitude of the two antagonistic wave fronts are observed. Fig. 3b illustrates the constructive interference between these two wave fronts to form two instantaneous local maxima regions of equal amplitude and apparently out of phase. The waves diverge from the source region, but two local maxima regions continues to be formed at the source regions, thereafter. It may however, be noted that the flux propagating out of the domain towards the LA (say, at the bottom boundary) interferes with the flux that emanates from this LA and propagates into the domain leading to formation of spurious local maxima regions near the computational boundary. This interference pattern may be observed in Fig. 3b at regions near the $y = \pm 0.5$ m boundaries. Hence, some further work has been carried out (Mimani *et al.*, 2013(b)) to eliminate this undesirable interference and spurious maxima regions which may affect the final result of TR simulation which is quantified by the following metric.

$$\tilde{p}_{\mathrm{RMS}}(i,j) = \sqrt{\frac{\sum_{k=1}^{k=\left(N_{\max}-N_{\mathrm{steady}}\right)} \tilde{p}^2\left(i,j,\tilde{t}=k\cdot\Delta t\right)}{\left(N_{\max}-N_{\mathrm{steady}}\right)}}, \qquad (11)$$

where, $\tilde{p}_{\mathrm{RMS}}(i,j) \equiv \tilde{p}\left(x=-L_x+(i-1)\Delta x,\ y=-L_y+(j-1)\Delta y\right)$ is the spatial distribution of Root-Mean-Square (RMS) of acoustic pressure field over the interval $\tilde{t} = \left[0, T_{\max} - T_{\mathrm{steady}}\right]$ and as shown by Padois *et al.* (2012), the location of time-harmonic aeroacoustic sources can be estimated by determining the region(s) of maximum in the $\tilde{p}_{\mathrm{RMS}}$ field. These regions of maximum RMS magnitude are called the focal spots. This method is based on the application of Sommerfeld radiation condition for 2-D free space, which states that the acoustic field consists of only the waves that propagate away from source towards infinity and their amplitudes decay as $1/\sqrt{r}$, whilst the acoustic intensity falls as r^{-1}, (Blake, 1986) where r is the distance from source.

Figures 4a and b depict the $\tilde{p}_{\mathrm{RMS}}$ field computed using the time-reversed acoustic pressure history of the idealised monopole source (simulated in Fig. 1a) from (a) one LA located at $y = 0.5$ m boundary and (b) two LAs located at $y = \pm 0.5$ m boundaries, respectively, wherein the known and predicted source locations are indicated by a circle **O** and a cross **X**, respectively. (The same sign conventions are followed for representing the known and predicted locations of the dipole sources in Figs. 5a and b, respectively.)

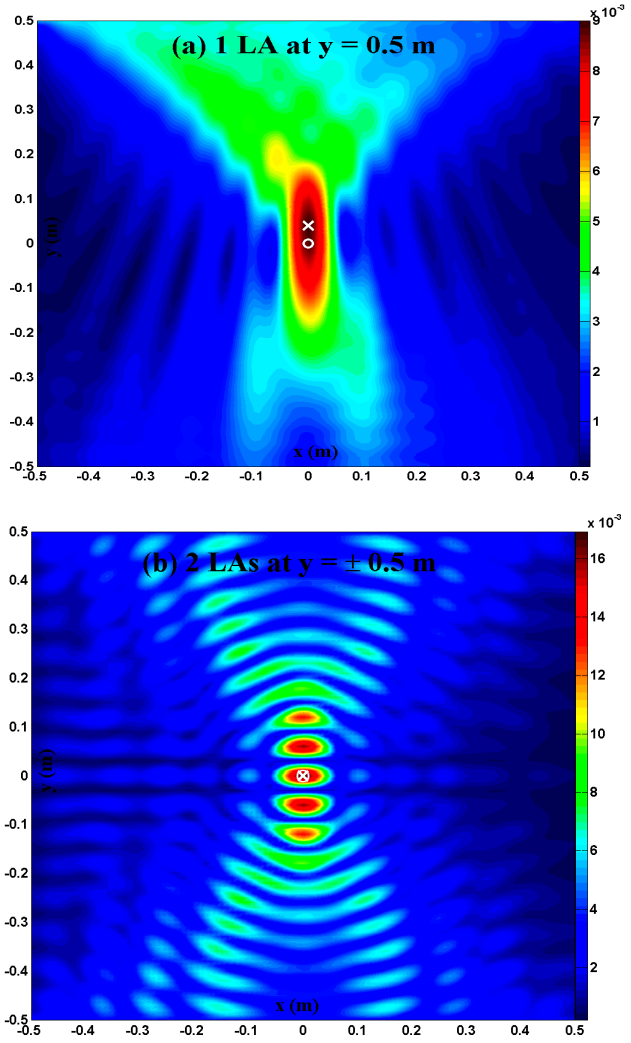

Figure 4 The $\tilde{p}_{\mathrm{RMS}}(i,j)$ field due to an idealised monopole source (3000 Hz) obtained by numerical TR simulations using (**a**) one LA located at y = 0.5 m boundary and (**b**) two LAs located at $y = \pm 0.5$ m boundaries.

The $\tilde{p}_{\mathrm{RMS}}$ field obtained using one LA shows an elongated focal spot located on the y axis between $-0.01\,\mathrm{m} \le y \le 0.09\,\mathrm{m}$ which is $0.87\lambda = 0.1$ m. As discussed in Rosny and Fink (2002), for a point monopole source, the focal spot size should be about $0.5\lambda = 0.06$ m using a LA configuration fully surrounding the source. The reason for focal spot size obtained in Fig. 4a being larger than 0.06 m is that only one LA is used. The monopole source location is nevertheless, estimated from the maxima of this focal spot (Padois *et al*., 2012) which is found at $x_m = 0, y_m = 0.04$ m, whereas the actual location of the source is at the origin. This discrepancy between the predicted and known source locations (clearly observed in Fig. 4a) is therefore, about 0.35λ. The $\tilde{p}_{\mathrm{RMS}}$ field obtained using two LAs located at $y = \pm 0.5$ m exhibits a central focal spot flanked by focal spots on the top and bottom of significantly lesser magnitudes as shown in Fig. 4b. This central focal spot is located at the x axis from $-0.03\,\mathrm{m} \le y \le 0.03\,\mathrm{m}$, therefore the decrease in its width (in comparison with the single LA) clearly indicates an improved resolution due to the use of two LAs. The monopole source location is predicted from the maximum of focal spot which is at $x_m = y_m = 0$, indicating that predicted

and known source locations are co-incident. The TR simulations were also implemented using two LAs located at $x = \pm 0.5$ m boundaries, wherein the $\widetilde{p}_{\mathrm{RMS}}$ field was found to be similar to that shown in Fig. 4b, except that flanking focal spots were located along the *x* axis. It may therefore, be concluded that prediction of monopole source location improves significantly with use of 2 LAs in a TRM. Indeed, the use of two LAs is necessary to confirm the monopole source nature. Also, the use of two LAs is able to recreate a larger fraction of the acoustic power (as back-propagating waves) to be refocused in the domain. Hence, predicted acoustic pressure amplitude of the monopole source (and also the focal energy spot) is greater in Fig. 4b in comparison to Fig. 4a.

Figures 5a and b depict the $\widetilde{p}_{\mathrm{RMS}}$ field of idealised dipole source with axis along the *y* direction (simulated in Fig. 1b) obtained using (a) one LA located at $y = 0.5$ m boundary and (b) two LAs located at $y = \pm 0.5$ m boundaries, respectively. The $\widetilde{p}_{\mathrm{RMS}}$ field obtained in Fig. 5a exhibits an elongated focal spot (identical to that obtained in Fig. 4a), therefore, incorrectly suggesting the presence of a monopole in the domain. The one LA located along the direction perpendicular to the axis of dipole source records only half the phase information. Therefore, owing to the small aperture size, the maximum resolution of one LA is limited, indeed, inadequate to properly resolve the dipole source characteristics. Nevertheless, the source location is found at $x_{s_1} = 0$, $y_{s_1} = 0.04$ m indicating a discrepancy of 0.35λ in the known location. The use of two LAs in Fig. 5b, however, indicates the presence of two focal spots (in proximity) of equal magnitude and offset on the *y* axis by a small distance at $x_{s_1} = 0, y_{s_1} = 0.03$ m, and $x_{s_2} = 0, y_{s_2} = -0.03$ m. Therefore, the use of two LAs in a TRM accurately predicts the presence of a dipole source. The geometrical centre of the two focal spots (termed as the focal points) at the origin is taken as the predicted dipole source location (Padois *et al.*, 2012). Hence, the predicted and known source locations are co-incident. It is noted that the aperture size doubles with use of two LAs, in fact, two LAs facing each other can record the minimum phase information to characterise a dipole source with axis perpendicular to the microphone LA comprising the TRM. Indeed, this increased resolution is crucial for resolving the difference between a monopole and a dipole source.

In order to confirm the dipole source nature, it must also be established that the two focal points (separated by a distance $d < \lambda$) in Fig. 5b are exactly out of phase with each other (Padois *et al.*, 2012). In other words, the relative phase ϕ between $\widetilde{p}\left(x_{s_1}, y_{s_1}, \widetilde{t}\right)$ and $\widetilde{p}\left(x_{s_2}, y_{s_2}, \widetilde{t}\right)$ at the two focal points s_1 and s_2 (during time-harmonic response) should be exactly π radian. To this end, two signals

$$\eta_1(t) = A_1 \sin(\omega t), \ \eta_2(t) = A_2 \sin(\omega t + \phi) \qquad (12, 13)$$

are considered, where A_1 and A_2 are the amplitudes and relative phase ϕ is related to the time-lag Δt_{lag} between the two coherent signals as

$$\phi = \omega \Delta t_{\mathrm{lag}} = \omega\left(t_1 - t_2\right), \qquad (14)$$

where $\eta_1(t_1) = \eta_2(t_2) = 1$, thereby signifying the same phase corresponding to nearest crests of the two signals. For the special case of $\phi = \pi$, $\eta_2(t) = -\kappa\,\eta_1(t)$, ($\kappa = A_2 / A_1$ being the scaling factor), therefore, the second signal may be simply obtained by reversing the sign and scaling the first signal. Figure 6 shows the variation of acoustic pressure histories $\widetilde{p}\left(x_{s_1} = 0, y_{s_1} = 0.03\,\mathrm{m}, \widetilde{t}\right)$ and $\widetilde{p}\left(x_{s_2} = 0, y_{s_2} = -0.03\,\mathrm{m}, \widetilde{t}\right)$ at the two focal points s_1 and s_2 over the reverse time-interval $\widetilde{t} = \left[0, T_{\max} - T_{\mathrm{steady}}\right]$ obtained using TR simulation using two LAs for the dipole source.

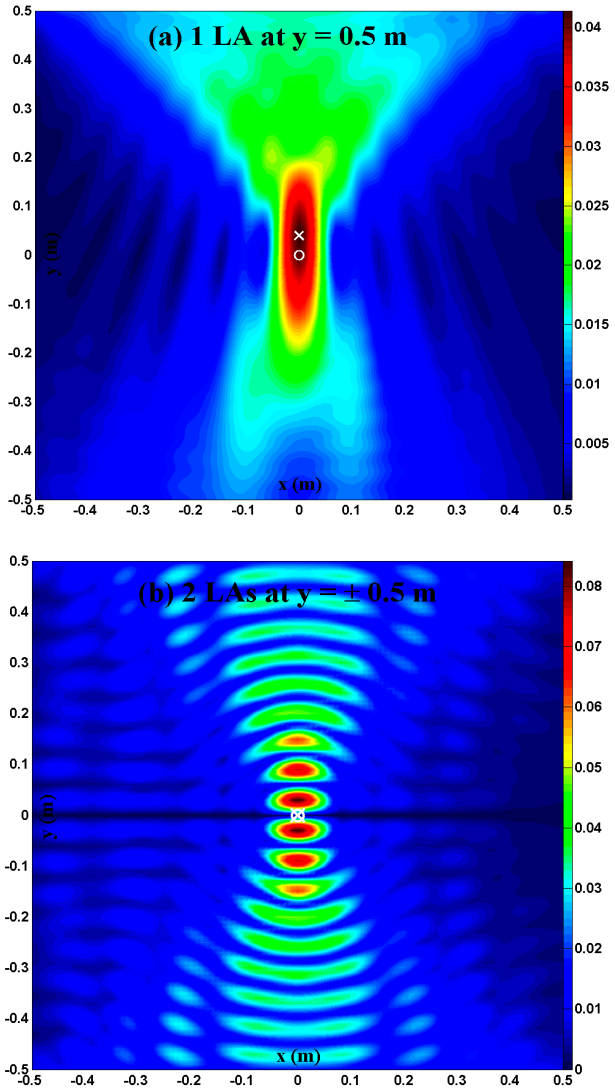

Figure 5 The $\widetilde{p}_{\mathrm{RMS}}(i, j)$ field due to an idealised dipole source (3000 Hz) with axis oriented along the *y* direction obtained by numerical TR simulations involving (**a**) one LA located at *y* = 0.5 m and (**b**) two LAs located at $y = \pm 0.5$ m.

It is observed that $\Delta t_{\mathrm{lag}} = 149\Delta t$ or $\phi \approx \pi$ radian. Indeed, the acoustic pressure histories, $-\widetilde{p}\left(x_{s_1} = 0, y_{s_1} = 0.03\,\mathrm{m}, \widetilde{t}\right)$ and $\widetilde{p}\left(x_{s_2} = 0, y_{s_2} = -0.03\,\mathrm{m}, \widetilde{t}\right)$ are co-incident throughout the duration of TR simulations, thereby indicating that the two focal points are coherent and have exactly opposite phase, thereby constituting a dipole source. Moreover, the time-snapshots of the TR simulations shown in Fig. 3b also demonstrate that acoustic pressure at regions near the two focal points at $\left(x_{s_1}, y_{s_1}\right)$ and $\left(x_{s_2}, y_{s_2}\right)$ are in opposite phase. Therefore, the dipole source nature may also be confirmed on basis of these observations.

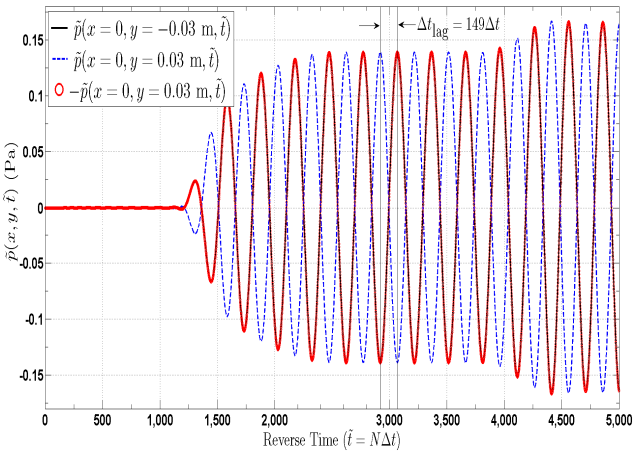

Figure 6 Comparsion of local $\tilde{p}(x, y, \tilde{t})$ time-history at the two predicted focal points s_1 and s_2 consituting the dipole source obtained by numerical TR simulations using two LAs located at $y = \pm 0.5$ m boundaries.

Equation (14) is used to compute the relative phase distribution $\phi(x, y)$ (shown in Fig. 7) over the region $|x| \le 0.05$ m, $|y| \le 0.05$ m enclosing the two predicted focal points s_1 and s_2 computed with respect to $\tilde{p}(x_{s_1} = 0, y_{s_1} = 0.03\,\text{m}, \tilde{t})$, i.e., the acoustic pressure time-history at the focal point s_1. (Hence, the relative phase $\phi = 0$ at the focal point s_1.)

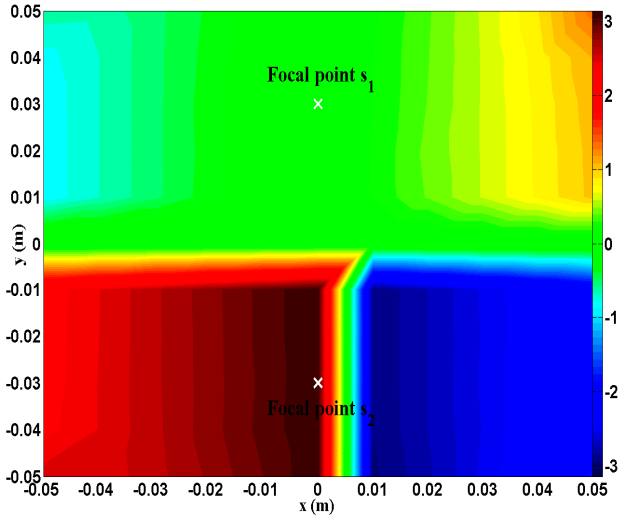

Figure 7 The phase distribution $\phi(x, y)$ (in radian) of local $\tilde{p}(x, y, \tilde{t})$ over the region $|x| \le 0.05$ m, $|y| \le 0.05$ m enclosing the two predicted focal points s_1 and s_2 (shown by a cross **X**) with respect to $\tilde{p}(x = 0, y = 0.03\,\text{m}, \tilde{t})$ at focal point s_1.

The objective is to analyse the variation in ϕ in vicinity of the focal points s_1 and s_2. The colour bar on right shows the $\phi(x, y)$ in radian. The most prominent feature of Fig. 7 is the near π phase jump in ϕ about the x axis (Padois *et al.*, 2012), signifying that two halves about x axis are basically out of phase. In particular, $\phi = \pi$ radian at the focal point region s_2, whilst the deviation from π phase gradually increases with an increase in distance from the focal point s_2 on either sides of the lower half region $y \le 0$, $|x| \le 0.05$. The $\phi(x, y)$ over the upper half region $y \ge 0$, $|x| \le 0.05$ gradually deviates from $\phi = 0$ (i.e., in phase oscillations) at the focal point s_1 with an increase in distance on either sides of this focal point.

CONCLUSIONS

The localisation and characterisation of idealised harmonic monopole and dipole aeroacoustic sources by means of numerical TR simulations using one LA and two LAs in a TRM has been examined. The use of one LA yields typically an error in predicted source location which is approximately of the order of λ. Furthermore, one LA cannot reveal the source characteristics. These limitations are attributed to the interception of acoustic waves on only one-quarter of the computational boundary, i.e. due to small aperture size of one LA. Regardless of the source characteristics, the use of two LAs in a TRM significantly reduces the error in predicted source location due to increased resolution characteristics. In fact, use of two LAs in a TRM is essential to obtain the minimum information (in terms of acoustic pressure time-history) to determine the nature of acoustic source. It has been shown that two LAs are sufficient to localise the two sources (in proximity) constituting a dipole source. Indeed, using two LAs, a monopole source nature is revealed if the $\tilde{p}_{\text{RMS}}$ field resembles Fig. 4b, whilst the $\tilde{p}_{\text{RMS}}$ field resembling Fig. 5b, suggests that the source is most likely a dipole source. The dipole source nature is confirmed by determining the relative phase ϕ between the two focal points (in proximity) indicated in the $\tilde{p}_{\text{RMS}}$ field. To this end, a simple method is used which is based on estimating the time-lag Δt_{lag} between two sinusoidal signals (of same frequency) when these signals are at same phase. Using this method, the coherent acoustic pressure time-histories at the two focal points in Figs. 5b are shown to have π phase difference, hence are exactly out of phase, thereby confirming the dipole source nature. Therefore, computation of Fast Fourier Transform (FFT) to obtain the phase distribution of acoustic pressure field over the entire domain (for estimating the relative phase between the two focal points) is avoided, resulting in a substantial reduction of computational effort. Nevertheless, in order to analyse the variation of relative phase in the vicinity of two predicted focal points, the phase distribution $\phi(x, y)$ has been computed over a small rectangular region enclosing the two predicted focal points. A near π phase jump observed about the geometrical location of dipole source indicates that two halves are basically out-of-phase.

The physical significance of the results of numerical simulations is to gain *a-priori* knowledge of the minimum number of microphone LAs in a TRM that would be required for localising and resolving a dipole source experimentally. For instance, the acoustic field generated by uniform cylinder located in a mean flow (with the cylinder axis being perpendicular to flow direction) in an aeroacoustic wind tunnel resembles that of a dipole source (Blake, 1986) with axis perpendicular to the flow direction (see Fig. 1b). Therefore, as shown here, acoustic pressure recorded over two LAs in a TRM at top and bottom boundaries is essential and indeed sufficient to accurately localise the sound source, (i.e., the cylinder) and also resolve the dipole source nature using numerical TR simulations. Indeed, the reason for using two LAs located along (and not perpendicular) to the mean flow direction is that the LA(s) should not be located within the flow region; hence, for flow in an anechoic wind tunnel, the two LAs may be positioned at the top and bottom boundaries.

The interference between the flux propagating out of the computational domain towards a LA and that propagating in the domain emanating from the same LA may result in formation of spurious local maxima at regions near the LA. Although, the numerical TR simulations involving two LAs in a TRM yield an accurate source location (and can also characterise a monopole and a dipole source), this interference of opposing fluxes near the LA(s) is likely to induce errors when multiple sources (of different characteristics) are present in the domain. Therefore, a numerical sponge layer technique has been developed in a further work (Mimani *et al*., 2013(b)) that damps the flux propagating towards a LA (at the first few nodes adjacent to the LA) whilst leaving the flux propagating away from the LA into the computational domain unaffected. This technique termed as the Time-Reversal Sponge Layer (TRSL) minimizes the interfence, thereby enhancing the $\widetilde{p}_{\mathrm{RMS}}$ field used to estimate the location and nature of sources.

Acknowledgements

The authors are grateful to Professor Vincent Valeau for useful suggestions and comments. This work was supported by the Australian Research Council under the project "Resolving the mechanics of turbulent noise production", grant number ARC DP 120102134.

REFERENCES

Bailly, C & Juve, D 2000, 'Numerical solution of acoustic wave propagation problems using linearized Euler equations', *AIAA Journal*, vol. 38, no. 1, pp. 22-29.

Bavu, E, Besnainou, C, Gibiat, V, Rosny, J de & Fink, M 2007, 'Subwavelength sound focusing using a time-reversal acoustic sink', *Acta Acustica United with Acustica*, vol. 93, no. 5, pp. 706-715.

Blake, WK 1986, *Mechanics of Flow-Induced Sound and Vibration*, Volume 1, Academic Press, New York.

Clayton, R & Engquist, B 1977, 'Absorbing boundary conditions for acoustic and elastic wave equations', *Bulletin of Seismological Society of America*, vol. 67, no. 6, pp. 1529-1540.

Deneuve, A, Druault, P, Marchiano, R & Sagaut, P 2010, 'A coupled time-reversal/complex differentiation method for aeroacoustic sensitivity analysis: towards a source detection procedure', *Journal of Fluid Mechanics*, vol. 642, no. 1, pp. 181-212.

Engquist, B & Majda, A 1977, 'Absorbing boundary conditions for the numerical simulation of waves', *Mathematics of Computation*, vol. 31**,** no. 139, pp. 629–651.

Engquist, B & Majda, A 1979, 'Radiation boundary conditions for acoustic and elastic wave calculations', *Communications in Pure and Applied Mathematics*, vol. 32, no. 3, pp. 313–357.

Fink, M, Cassereau, D, Derode, A, Prada, C, Roux, P, Tanter, M, Thomas, JL & Wu, F 2000, 'Time-reversed acoustics', *Reports on Progress in Physics*, vol. 63, no. 12, pp. 1933-1995.

Fink, M & Prada, C 2001, 'Acoustical time-reversal mirrors', *Inverse Problems*, vol. 17, no. 1, R1-R38.

Harker, BM & Anderson, BE 2013, 'Optimization of the array mirror for time reversal techniques used in half-space environment', *Journal of Acoustical Society of America – Express Letters*, vol. 133, no. 5, EL351-EL357.

Li, Y 1997, 'Wavenumber-extended high-order upwind-biased finite-difference schemes for convective scalar transport', *Journal of Computational Physics*, vol. 133, no. 2, pp. 235-255.

Lu, S-Yi & Sagaut, P 2007, 'Pseudo-characteristic formulation and dynamic boundary conditions for computational aeroacoustics', *International Journal of Numerical Methods in Fluids*, vol. 53, no. 2, pp. 201-227.

Mimani, A, Doolan, C, J & Medwell, P, R 2013(a) 'Application of compact upwind biased finite difference schemes for 2-D time reversal simulations', in Proceedings of the 20th *International Congress on Sound and Vibration* (7th to 11th July, Bangkok, Thailand).

Mimani, A, Doolan, C, J & Medwell, P, R 2013(b) 'Multiple line arrays for the characterization of aeroacoustic sources using a time-reversal method', *Journal of Acoustical Society of America – Express Letters*, vol. 134, no. 4, DOI: 10.1121/1.4819185.

Padois, T, Prax, C, Valeau, V & Marx, D 2012, 'Experimental localization of an acoustic source in a wind-tunnel flow by using a numerical time-reversal technique', *Journal of Acoustical Society of America*, vol. 132, no. 4, pp. 2397-2407.

Rosny, J de & Fink, M 2002, 'Overcoming the diffraction limit in wave physics using a time-reversal mirror and a novel acoustic sink', *Physical Review Letters*, vol. 89, no. 12, 124301.

Sesterhenn, J 2001, 'A characteristic-type formulation of the Navier-Stokes equations for high order upwind schemes', *Computers and Fluids*, vol. 30, no. 1, pp. 37-67.

Shu, C-W & Osher, S 1988, 'Efficient implementation of essentially non-oscillatory shock capturing scheme', *Journal of Computational Physics*, vol. 77, no. 2, pp. 439-471.

Tam, CKW 1995, 'Computational aeroacoustics: issues and methods', *AIAA Journal*, vol. 33, no. 10, pp. 1788-1796.

Tam, CKW & Webb, JC 1993, 'Dispersion-relation-preserving finite-difference schemes for computational acoustics', *Journal of Computational Physics*, vol. 107, no. 2, pp. 262-281.

Zhuang, M & Chen, RF 2002, 'Applications of high-order optimized upwind schemes for computational aeroacoustics', *AIAA Journal*, vol. 40, no. 3, pp. 443-449.